The detection of tumor sub-regions based on T_1 and ADC clustering

C. Roberts[1,2], C. Rose[1,2], J. H. Naish[1,2], Y. Watson[1,2], S. Cheung[1,2], G. A. Buonaccorsi[1,2], G. C. Jayson[3], J. C. Waterton[2,4], J. Tessier[4], and G. J. Parker[1,2]

[1]Imaging Science and Biomedical Engineering, School of Cancer and Imaging Sciences, The University of Manchester, Manchester, United Kingdom, [2]The University of Manchester Biomedical Imaging Institute, The University of Manchester, Manchester, United Kingdom, [3]Cancer Research UK Dept Medical Oncology, Christie Hospital and University of Manchester, Manchester, United Kingdom, [4]AstraZeneca, Alderley Park, Macclesfield, Cheshire, United Kingdom

Introduction Tumors are known to be heterogeneous and often appear to have distinct sub-regions. However, tracer kinetic model-based analyses of dynamic contrast-enhanced (DCE)-MRI data typically report summary statistics, such as median K^{trans}, which treat tumors as being homogeneous. Anti-angiogenic therapies often preferentially affect certain tissue types and there is interest in the development of methods to provide insight into regional changes, such as techniques to sub-divide tumors into distinct regions (e.g., necrotic and viable tumor regions[1]). We present a method for identifying distinct tumor regions based on relaxation time and water diffusion measurements, based on the hypothesis that these parameters should be sensitive to alterations in tumor microenvironment that relate to the compartmentalization of water. The key insight is that there is clear structure to the joint distribution of voxel-wise estimates of the longitudinal relaxation time (T_1) and the apparent water diffusion coefficient (*ADC*); when clustered, this structure in the distribution of these parameters corresponds to clear spatial structure within tumors (see Figs 1a & b). More specific summaries can then be obtained, for example by limiting the computation of median K^{trans} to tumor sub-regions that are known to be relatively homogeneous according to T_1 and *ADC*.

Method *Imaging:* Eleven patients with confirmed ovarian cancer (stages IIc–IV) were recruited. Each patient was imaged before and after chemotherapy. DCE-MRI and DWI images were acquired using a Philips 1.5 T Intera (Philips Healthcare, Best, The Netherlands). The DCE-MRI protocol used an axial 3-D spoiled gradient echo (FFE/SPGR) sequence with baseline T_1 measured using the variable flip angle method with the following parameters: 2°, 10° and 20° flip angles, TR/TE = 4.0/0.92 ms, FOV = 375 x 375 mm, matrix = 128 x 128, slices = 26, thickness = 4 mm. The dynamic image acquisition used the same parameters with a flip angle of 20°, 75 dynamic timepoints and a temporal resolution of 5 s. On the sixth dynamic timepoint, 0.1 mmol/kg of body weight of 0.5 mmol/ml Omniscan (GE Healthcare) was administered through a Spectris power injector (Medrad Inc.) at a rate of 3 ml/s followed by an equal volume of saline flush also at 3 ml/s. DW images were acquired using a non-breath hold fat-supressed spin-echo EPI sequence with FOV = 375 x 375 mm, matrix = 142 x 142, slices = 26, thickness = 4 mm with b = 50, 400, 800, TR/TE = 3900/76 ms with 5 signal averages.

Data Analysis: A total of 15 tumors were included in the analysis. Regions of interest (ROI) were defined for the whole tumor volume. Enhancing voxels were identified and the extended Kety model[2] was fitted to each voxel's time series using an automated arterial input function extraction method[3]. 3D maps of T_1, the endothelial transfer constant (K^{trans}), the fractional extracellular extravascular space (EES, v_e), and the blood plasma volume (v_p) were estimated. Voxel-wise estimates of *ADC* were calculated using the same ROIs, by fitting to $S(b)=S_0e^{-b*ADC}$. All *ADC* maps were co-registered with DCE-MRI. Tumor sub-regions were identified by applying *k*-means clustering—with *k*=3—to the pooled group T_1 and *ADC* voxel data using MATLAB (The MathWorks, Natick, MA, USA). A cluster image was generated for each tumor and DCE-MRI parameters were calculated for each sub-region. Tumors that were predominantly cystic (as determined on high resolution T_2-weighted images) were excluded from the clustering.

Results The *k*-means clustering process separated voxelwise T_1 and *ADC* data into high T_1/low *ADC*, low T_1/low *ADC* and low T_1/high *ADC* regions (Fig. 1a). The spatial distribution of these clustered voxels can be seen in example tumor cluster maps (single slice) in Fig. 1b and demonstrates where the clustering process has sub-divided each tumor into distinct sub-regions. K^{trans} (min^{-1}), v_e, v_p and $IAUC_{60}$ (mM.s), calcuated within cluster 1 (the core of the tumor), show differences to clusters 2 and 3 and the overall group mean (Fig. 1c).

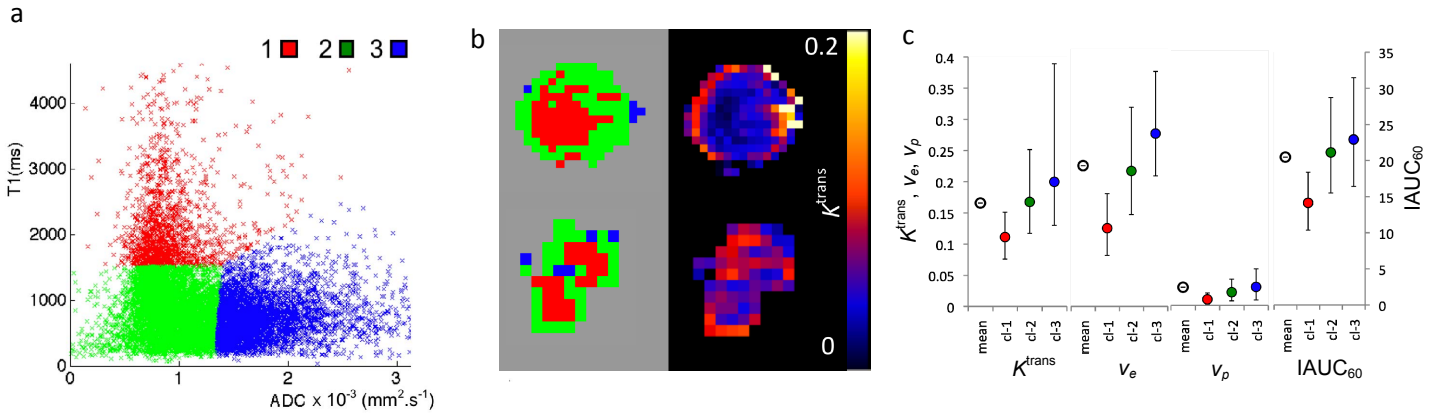

Figure 1: (a) Scatter plot of voxelwise *ADC* and T_1 pooled to include 15 tumor data sets. (b) *k*-means cluster maps for 2 example tumors and the corresponding K^{trans} (units = min^{-1}) maps. (c) Group (N=15) median DCE-MRI parameters calculated from each cluster (closed circles), error bars represent the 25th and 75th quartiles. Open circles represent the group mean of each tumor median calculated over the whole tumor volume.

Discsussion The observed relationship between T_1 and *ADC* has enabled the clustering of clear tumor sub-regions and shows areas of high tumor activity, for example the tumor rim (green and blue regions in Fig. 1b) and lower tumor activity, such as the tumor core (red regions in Fig. 1b). Importantly, DCE-MRI parameters calculated from these sub-regions (Fig. 1c) show clear differences, particulary in the tumor core (red region in Fig. 1b). This method may offer the potential to monitor changes in distinct tumor regions rather than relying on tumor-wise summary statistics that assume tumors to be homogeneuos. The use of parameters that are unlikely to be related to microvascular function reduces the likelihood of bias in the selection of tumour sub-regions, which may be of benefit in the objective assessement of intra-tumor heterogeneity.

References **1.** Berry LR et al. Magn Reson Med 2008;60(1):64-72. **2.** Tofts PS. J Magn Reson Imaging 1997;7(1):91-101. **3.** Parker GJ et al. Magn Reson Med 2006;56(5):993-1000.